Biophysical Journal
Article

Biophysical Society

Dynamic Scaling Analysis of Molecular Motion within the LAT:Grb2:SOS Protein Network on Membranes

William Y. C. Huang,[1] Han-Kuei Chiang,[1] and Jay T. Groves[1,*]
[1]Department of Chemistry, University of California, Berkeley, Berkeley, California

ABSTRACT Biochemical signaling pathways often involve proteins with multiple, modular interaction domains. Signaling activates binding sites, such as by tyrosine phosphorylation, which enables protein recruitment and growth of networked protein assemblies. Although widely observed, the physical properties of the assemblies, as well as the mechanisms by which they function, remain largely unknown. Here we examine molecular mobility within LAT:Grb2:SOS assemblies on supported membranes by single-molecule tracking. Trajectory analysis reveals a discrete temporal transition to subdiffusive motion below a characteristic timescale, indicating that the LAT:Grb2:SOS assembly has the dynamical structure of a loosely entangled polymer. Such dynamical analysis is also applicable in living cells, where it offers another dimension on the characteristics of cellular signaling assemblies.

INTRODUCTION

The assembly of cellular proteins into organized structures through modular binding domains is a broadly significant theme in biological signal transduction (1,2). Hallmark examples include P granules (3), the nuclear pore complex (4,5), receptor tyrosine kinases (6), actin cytoskeleton regulation (7,8), and immune cell receptor signaling (2,9–11). Common to all of these systems are multivalent protein-protein interactions, such as SH2 domain binding to phosphorylated tyrosine (pY) residues, SH3 domain binding to proline-rich regions, and interactions between FG-rich repeat domains (5,8,9). Multivalency enables networked assembly of proteins into extended structures via bond percolation (Fig. 1). In a number of cases, assembly is reversibly governed by tyrosine phosphorylation, which is one of the primary mechanisms of transmitting information in signal transduction cascades (1). Various functional consequences of such assemblies in signal transduction have been envisioned (10,11). However, detailed understanding of their physical properties as well as how these modulate the molecular logic of signaling remains vague.

Extensive networks of weak and rapidly reversible (e.g., ~500 ms for SH2:pY) interactions have manifested in both 2D and 3D apparent phase transitions in reconstituted systems (7,8,10,11). The static connectivity of molecular assembly is analogous to a polymer, and assembly formation has been proposed to exhibit a gelation phase transition (12) (a transition in connectivity in which a polymer can proliferate into an infinite network (13,14)). Alternatively, the rapid turnover of individual molecules within the assembly, along with the visible macroscopic physical property of surface or line tension, has led to their description as viscous fluids (3,8). These different possibilities have distinct dynamical properties with correspondingly different potential effects on chemical kinetics of signaling reactions. Detailed examination of the dynamic scaling of molecular mobility offers one approach to determine the molecular-scale structural identity of the assembly. In particular, the dynamical scaling law, defined as k in $\langle r^2 \rangle \propto t^k$, where r is distance traveled by an individual molecule (13), is an experimentally measurable property relating to both molecular structure as well as the diffusion process within the biochemical reaction itself. The dynamical scaling law exhibits different characteristics for gels (13), viscous fluids (15), and other forms of molecular organization.

In this study, the translational motion of individual LAT proteins engaged in the LAT:Grb2:SOS networked molecular assembly on supported membranes is comprehensively studied by single-molecule tracking. LAT is a scaffold protein in the T cell receptor signaling system with nine

Submitted April 19, 2017, and accepted for publication August 14, 2017.
*Correspondence: jtgroves@lbl.gov
Editor: Joseph Falke.
http://dx.doi.org/10.1016/j.bpj.2017.08.024

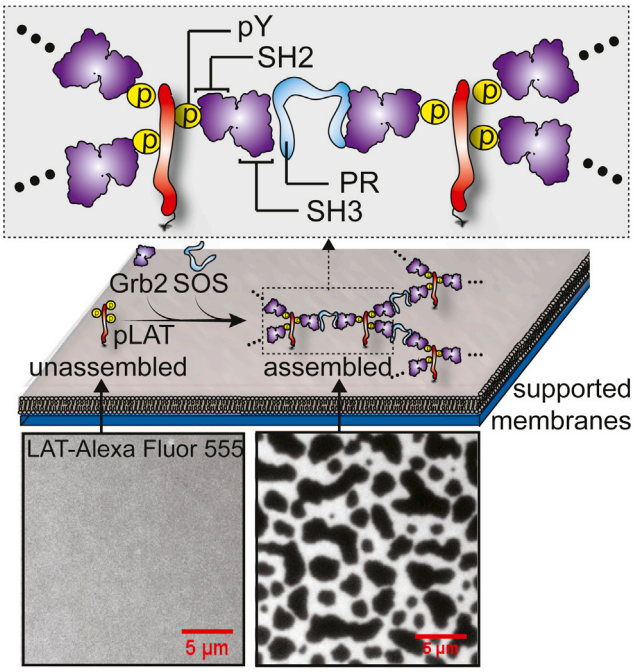

FIGURE 1 Molecular assembly of LAT:Grb2:SOS by bond percolation. These bonds are transient and reversible modular protein-protein interactions (*inset*). Membrane-anchored LAT is cross-linked by membrane-recruited cytosolic proteins, Grb2 and SOS. The probability of cross-linking adjacent LAT is determined by the binding kinetics between each molecular species. The dissociation constants of SH2:pY and SH3:PR (proline-rich domain) are ~300 and 400 nM, respectively (9). In the reconstitution experiments, addition of Grb2 and SOS in solution drives LAT assemblies on supported membranes. The images of fluorescently labeled LAT (Alexa Fluor 555) are shown before (*bottom*, *left*) and after (*bottom*, *right*) assembly.

tyrosine residues, three of which are known to recruit Grb2 after phosphorylation (9,16). Activation of T cell receptors by ligand leads to activation of the Zap70 kinase, which phosphorylates LAT. This occurs against a background of LAT dephosphorylation by phosphatase activity. The overall degree of LAT phosphorylation is dynamically regulated by this kinase-phosphatase balance, which ultimately tunes the threshold for propagating a signal from the T cell receptor to downstream components of the signaling pathway. Phosphorylation of LAT then leads to LAT assemblies mediated by interactions with multivalent cytosolic proteins such as Grb2 and SOS. Grb2 contains SH2 and SH3 domains, enabling it to simultaneously bind pY residues on LAT and the proline-rich region on SOS. SOS can bind to at least two Grb2 molecules, enabling extended network assembly as long as the LAT proteins are sufficiently phosphorylated (Fig. 1). This phosphotyrosine-mediated network assembly was initially proposed based on cellular imaging experiments (9) and subsequently analyzed theoretically (12). Recently, a reconstitution approach with purified proteins and artificial membranes was developed to provide a well-controlled system (10,11) for detailed examination of the molecular identity of LAT assembly. Here we take advantage of this approach in combination with single-molecule tracking to analyze the dynamical structure of LAT assembly.

Phosphorylated LAT proteins reconstituted on supported membranes are laterally fluid and coalesce into assembled structures upon addition of Grb2 and SOS. This phase transition is reversible by addition of phosphatase and the structure is dynamically controlled by the degree of LAT phosphorylation (10,11). We measure the dynamical scaling law of LAT movement on membranes and observe subdiffusive motion ($\langle r^2 \rangle \propto t^k$, where $k < 1$) of LAT in the assembly only below a characteristic timescale. Multiple subdiffusive timescales can be resolved with faster image acquisition rates. Comparing these results with Monte Carlo simulations and classical polymer theory reveals that the LAT:Grb2:SOS networked assembly has a dynamical structure similar to a loosely entangled polymer.

MATERIALS AND METHODS

This section is detailed in Supporting Material (11,13,17–26).

RESULTS AND DISCUSSION

Diffusion analysis of LAT molecules within LAT:Grb2:SOS assemblies

We reconstituted the LAT:Grb2:SOS assembly on supported membranes using the cytoplasmic domain (residues 30–233) of LAT with an N-terminus 6-His tag, which was chelated onto DOPC bilayers containing 4% Ni-NTA lipids (Fig. 1) (11,23). Typical LAT densities on the membrane surface for these experiments, measured by fluorescence correlation spectroscopy (26,27), were ~2400 molecule/μm^2. LAT was phosphorylated by inclusion of dilute Src family kinase, Hck, on membranes (typically with densities of <100 molecule/μm^2). No phosphatase was included in these experiments, thus LAT is fully phosphorylated, as inferred from the extent of Grb2 recruitment (11). Under these experimental circumstances, Hck kinase activity is indistinguishable from Zap70, and corresponds to the physiological situation of strong receptor activation (11). Single-molecule trajectories from individual LAT molecules were tracked by labeling a trace fraction (~0.1%) with Alexa Fluor 555 fluorescent dye and imaging on a total internal reflection fluorescence microscopy setup.

In the absence of assembly, single-molecule trajectories of LAT on the supported membrane reveal simple diffusive motion, with a linear scaling of mean-squared displacement (MSD) with time (Fig. 2 *A*). MSD analysis is performed on each time trajectory of positions, $\{x(t), y(t)\}$, by the time-averaging protocol: $MSD(n\delta t) = 1/(N-n-1)\sum_{j=1}^{N-n-1} \{[x(j\delta t + n\delta t) - x(j\delta t)]^2 + [y(j\delta t + n\delta t) - y(j\delta t)]\}^2$, where δt is the time between frames, N is the total number of frames in a single trajectory, and n and j are positive integers

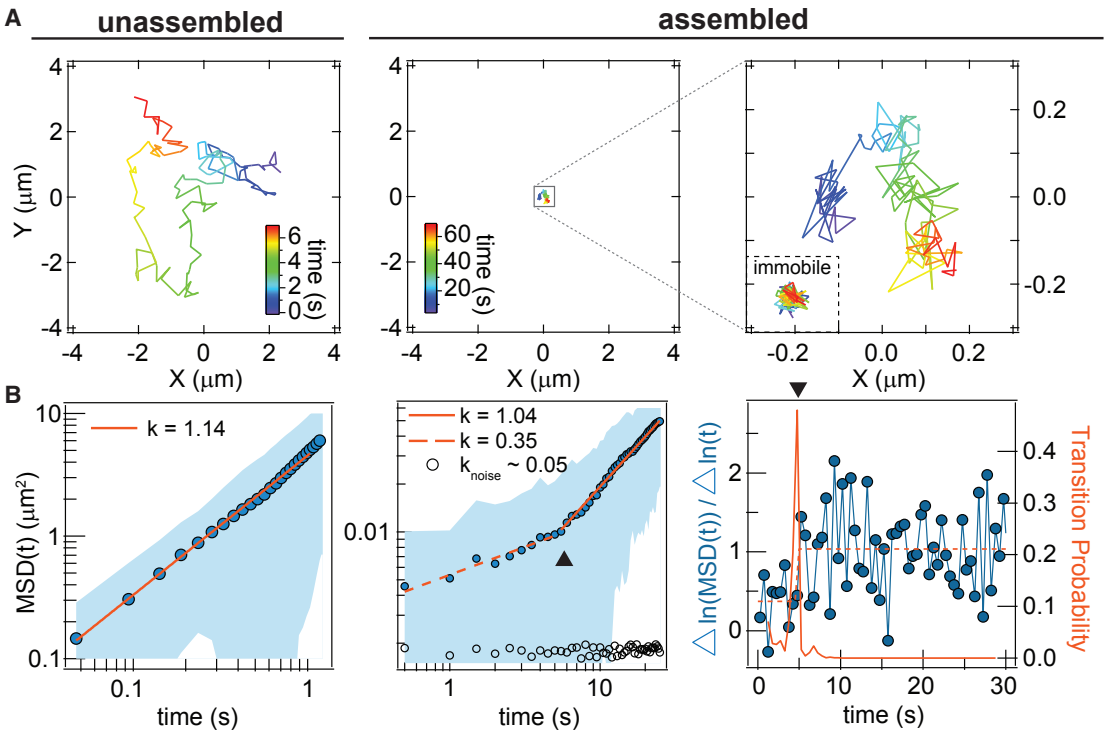

FIGURE 2 Dynamic scaling of LAT:Grb2:SOS assembly. (*A*) Single-molecule tracking of dilute labeled LAT before and after assembly. The time axis is color-coded in the trajectory. The inset of the right plot shows a trajectory of an immobilized LAT particle on a glass substrate tracked under identical imaging conditions, to quantify the extent of instrumental noise (*circles* in (*B*)). (*B*) Time-averaging MSD analysis for the trajectories in (*A*), fitted to a power law in a log-log plot. The fitted A for $k = 1.14$, 1.04, and 0.35 are 4.5, 0.0017, and 0.0054, respectively. The shaded area is the SD calculated from a single trajectory. The characteristic timescale (*triangle*) is estimated with a Bayesian change-point algorithm (*right*). Analysis in (*B*) is applied to the same trajectory shown in (*A*).

(21). MSD traces from single trajectories >100 frames were analyzed in terms of a power law, $MSD(t) = At^k$. For unassembled LAT on the supported membrane, fitted values of k were around unity over all timescales, indicating simple Brownian motion. In this case, the diffusion coefficient (D) is well defined and $A = 4D$ for 2D motion. Fit values of D were ~1–1.5 $\mu m^2/s$ (Fig. 2 *B*), which are typical for a monomeric protein on supported membranes (26,27).

To trigger networked assembly of LAT, Grb2 and the proline-rich domain of SOS were added in the solution at 5.8 and 1.45 μM, respectively. We take advantage of the reconstitution approach to use a higher concentration of proteins to drive the formation of stable and extended LAT assembly of sufficient size (~μm) for single-molecule tracking (Fig. 1). Smaller submicron LAT assemblies formed within minutes can also be achieved by tuning the protein concentrations (10). Single-molecule dwell time analysis suggests that assemblies of different sizes exhibit similar kinetic features (11), suggesting that LAT assemblies are similar regardless of their sizes. Under this basis, we drive the reconstituted system to extended LAT:Grb2:SOS network assemblies formed over the course of ~30 min, after which the system reaches a semistationary state (Fig. 2 *A*). The micron-size assemblies are spatially convenient for single-molecule characterization of dynamics within LAT assemblies.

Single-molecule imaging of LAT in the assembled state, acquired at a relatively slow frame rate of 2 Hz, reveals highly constrained and localized motion (Figs. 2 *A* and S1; Movie S1). This slow acquisition strategy allows individual molecules to be tracked for 100 s before photobleaching. MSD analysis shows that below a characteristic timescale of a few seconds, LAT is subdiffusive ($k \sim 0.1$–0.4). Over longer time intervals, linear scaling of MSD with time ($k \rightarrow 1$) is restored, albeit with slow diffusion coefficients of <0.01 $\mu m^2/s$ (Fig. 2 *B*). The characteristic timescales are determined using a Bayesian change-point algorithm (20) to evaluate if and where transition occurs (Supporting Materials and Methods). Observations over many trajectories confirm that the transition between subdiffusive and normally diffusive motion exists in the time domain only, all tracked molecules reside within the LAT gel, and mobility is spatially homogeneous. Membrane-bound Grb2 and SOS (imaged with dilute Alexa Fluor 647-labeled construct) also exhibit similar transitions from subdiffusive to diffusive dynamics on short timescales (Fig. S2). Errors from tracking due to instrument stability and the tracking algorithm are assessed using LAT molecules immobilized directly on glass surfaces. Immobile molecules result in weak power dependence ($k < 0.1$), low amplitudes of <0.003 μm^2, and absence of a characteristic

transition timescale within 100 s (Fig. 2). Therefore, we conclude that the observed transitions are dominated by genuine molecular motion.

Time-dependent subdiffusion of LAT is similar to the viscoelastic motion of a polymer

The binding relationship of LAT:Grb2:SOS hints that the assemblies can maintain an effective structure of a polymer (13,28). However, the reversibility of the bonds introduces an additional layer of dynamics different from a conventional polymer (29). We first compare the basic feature of experimental observation, the subdiffusion-to-diffusion motion, with Monte Carlo simulations of random walks (13,17,19,25) on 2D lattices. The role of the simulations, together with the accompanying discussion of classical literature in polymer physics, are meant to help evaluate how different subdiffusion mechanisms may be distinguishable in experimentally acquired MSD analyses. We specifically compare polymer bonding to two other commonly described subdiffusion mechanisms of membrane proteins—confinement from compartmentalization (30) and crowding effects (31). A purely random walk on a lattice yields a scaling of $k \rightarrow 1$ (Fig. 3 *A*). Simple polymer constraints (see Supporting Materials and Methods) (13,17,19) recreate subdiffusive motion over short timescales whereas diffusive motion is observed on longer timescales (Fig. 3 *A*). Confinement by an impassable square box results in a plateau in the MSD curve (Fig. 3 *B*). Crowding effects are considered by trapping of molecules with a heavy-tail waiting time. In this case, the ensemble MSD follows subdiffusion whereas MSD from individual trajectories does not exhibit subdiffusion (Fig. 3 *C*); (18,25). Although there can be other possible microscopic crowding mechanisms, we exclude trapping of proteins in a dynamic crowding environment as the reason for the observed subdiffusion.

The LAT:Grb2:SOS assembly does not form a conventional polymer. It differs by the fact that individual bonds are rapidly forming and breaking and some of the system dynamics result from these bond rearrangements (29). The bond dynamics themselves will increase the overall molecular turnover within the system as individual molecules may join and exit the assembly or move within it via a bind-unbind-rebind mechanism. However, random binding to and escaping from immobile sites alone is insufficient to cause subdiffusion on any characteristic timescale (Fig. 3 *D*; Supporting Materials and Methods). Binding to and escaping from a mobile polymer network (Supporting Materials and Methods) recreates the time-dependent subdiffusion with increased mobility, but the characteristic timescale depends on the relative timescale between the bond lifetimes and polymer constraints—the faster timescale will determine the value of the characteristic timescale (Fig. 3 *E*) (29). In the case of LAT, the effective bond lifetime depends on simultaneous breakage of all multivalent interactions (Fig. 1), which is estimated to be >10 s (11). Given that the observed characteristic timescales are 1–10 s (Figs. 2 and S1), this corresponds to the scenario where mean bond breakage time exceeds polymer relaxation time such that the dominating motion is then that of polymer constraints. This is further supported by the observation that Grb2 and SOS trajectories (which are terminated when the molecule escapes the assembly) both show similar characteristic transition timescales (Fig. S2). Bond rearrangements may facilitate the overall mobility. Taken with the evidence that the modular domains of LAT:Grb2:SOS (9) can form aggregated assemblies (12), the experimentally observed dynamical scaling of LAT mobility within the condensed assembly best resembles the viscoelastic motion of a polymer. Additional evidence emerges when imaging LAT motions with faster acquisitions and comparing with classical polymer theory.

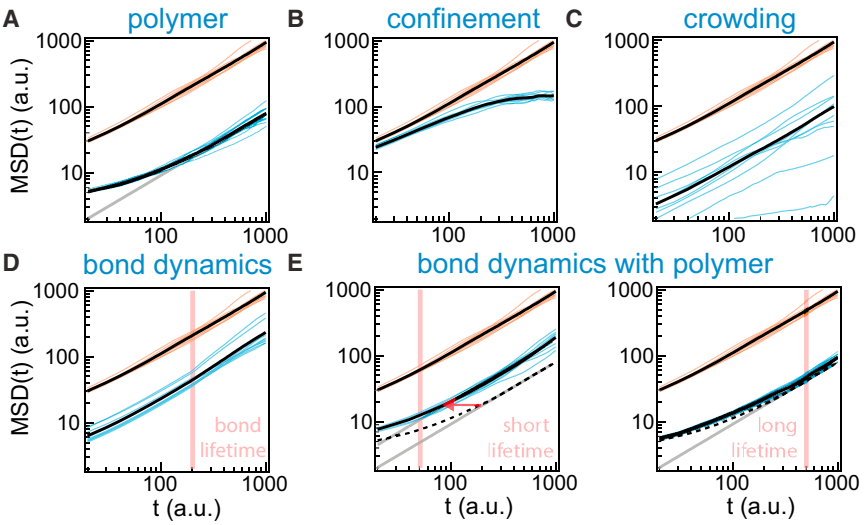

FIGURE 3 Time-averaging MSD from Monte Carlo simulations of 2D random walk. Molecular motions are constrained by (*A*) polymer bonding, (*B*) confinement, (*C*) crowding effect, (*D*) binding to immobile sites, and (*E*) binding to polymers. Orange (*upper*, faster) and blue (*lower*, slower) curves correspond to 10 simulated trajectories by the Brownian and the labeled mechanisms, respectively. Black curves are the averaged values. Gray curves are guidelines for linear scaling of MSD with time. Dashed lines in (*E*) are references to pure polymer constraints in (*A*). Pink vertical lines denote the bond lifetimes of the molecule binding to an immobile site or a polymer. In (*C*) and (*D*), the MSDs for the associated mechanisms are multiplied by a factor of 10 for clarity. To see this figure in color, go online.

A

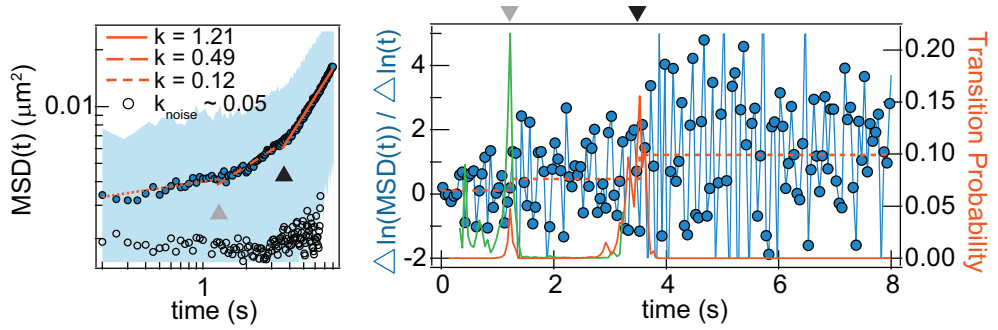

B

The reptation model		observed characteristic timescales
The reptation time	$\tau_{rep} = 6\tau_0 N_e^2 (N/N_e)^3$	5.1 ± 3.2 s
The Rouse time	$\tau_R = \tau_0 N^2$	0.64 ± 0.58 s
The Rouse time for an entangled strand	$\tau_e = \tau_0 N_e^2$	not observed (< 100 ms)

FIGURE 4 Multiple subdiffusive timescale. (*A*) MSD analysis of LAT mobility was acquired at a frame rate of 21 Hz. The shaded area is the SD of statistics from a single trajectory. Each timescale is fitted by a power law, with the characteristic timescales denoted by triangles. The fitted *A* for $k = 1.21$, 0.49, and 0.12 are 0.021, 0.011, and 0.0041, respectively. The orange and green curves of the right plot correspond to the transition probability calculated from the full timescale and the partial timescale before the slower (*black triangle*) characteristic timescale, respectively. (*B*) Given here is a comparison of the relaxation timescales between LAT assembly and the reptation model. The value τ_0 is the relaxation time of a monomer (not determined from experiments). The symbol ± denotes the SD. Statistics for the reptation and the Rouse time are both $n = 32$. To see this figure in color, go online.

Multiple time-dependent subdiffusion of LAT: entanglement within molecular assemblies

In experimental trajectories imaged at a 21-Hz frame rate, multiple relaxation timescales can be resolved for LAT motion within the assembly ($k_1 \sim 0.1$, $k_2 \sim 0.4$) (Fig. 4 *A*). This provides evidence for effective entanglement. The viscoelastic motion of a polymer arises from its relaxation modes, first analytically calculated by Rouse (28) and expanded to entangled polymers by Degennes (32). Entanglement of polymers in a condensed phase describes network chains imposing topological constraints to each other, promoting timescales of different subdiffusive dynamics (13). The reptation model for entangled linear polymers predicts multiple timescales of subdiffusion due to neighboring bond and topological constraints. In order of increasing timescale, these can be broken down as the Rouse time of an entangled strand (τ_e), the Rouse time (τ_R), and the reptation time (τ_{rep}). For LAT assemblies, the average number of bonds at a given time is most likely between 2 and 3 (LAT has a multivalency of three for Grb2, whereas each bond has a subsecond lifetime) (11,16). To gain some estimations of the entanglement effects, we compare the single-molecule data with the reptation model (13), which assumes effective bonds of two; the result is summarized in Fig. 4 *B*. Assignment of the observed timescales to the model is established by first recognizing that only the reptation time exhibits a temporal transition from subdiffusive to diffusive motion, whereas the Rouse time defines a transition between subdiffusive motions with different characteristic scaling. The observed scaling follows the prediction of the reptation model ($k_{\tau_R > t > \tau_e} < k_{\tau_{rep} > t > \tau_R} < k_{t > \tau_{rep}} \approx 1$). Although the original reptation model is considered in the case of 3D, the reptation motion itself is confined in 1D—the polymer occupies and moves in a snakelike motion along a tube (13). This effective entanglement is maintained in the case of LAT assemblies (Fig. 4), which is most likely structured in a quasi-2D geometry.

For an ideal polymer, the timescale of relaxation is determined by the longest relaxation mode, which reflects the total size and entanglement of the polymer strand (13). Within the 38 × 38 μm field of view, the distribution of observed relaxation timescales for individual trajectories within the LAT assembly is broad ($\tau_{rep} = 5.1 \pm 3.2$, $\tau_R = 0.64 \pm 0.58$ s) (Fig. 4 *B*). In some trajectories, subdiffusion persists without a characteristic transition timescale, indicating the existence of larger local assemblies. LAT assemblies of different sizes evidently coexist. Averaging the measurements provides estimations about the mean extent of connectivity within the assembly. The relative size of entanglement, N/N_e, where N_e is the number of monomers in an entangled strand and N is the total number of monomers in the polymer, is ~1–5 for LAT assembly (Fig. 4 *B*; Supporting Materials and Methods), suggesting a rather loose entanglement. The unobserved τ_e is estimated to be ~100 ms, which is at the limits of our MSD analysis resolution.

LAT gelation

Based on the multivalent interactions of LAT, the assemblies have been suggested to resemble a gelation phase transition

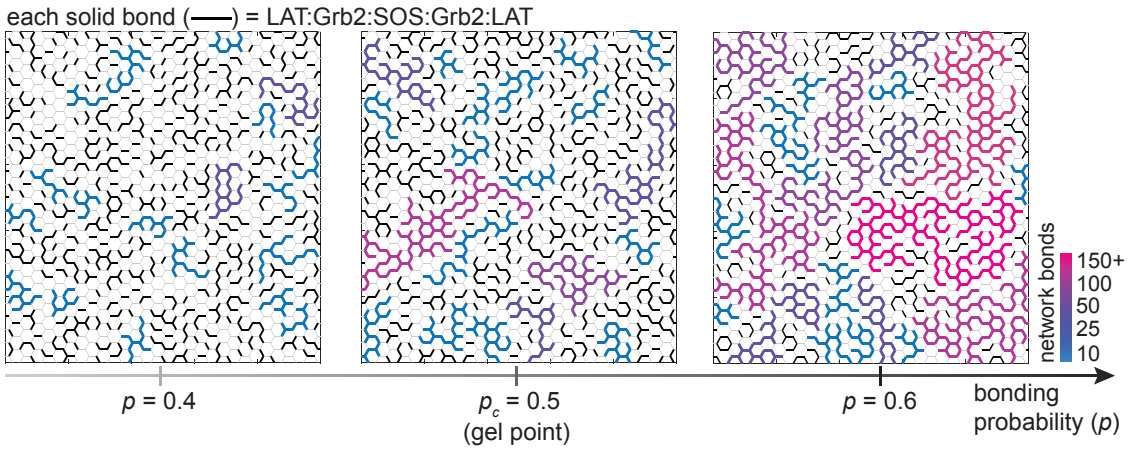

FIGURE 5 LAT gelation. LAT has a minimum multivalency of three, which can be represented by honeycomb lattices. Each intersection represents a LAT molecule, whereas each edge represents a possible bond of LAT:Grb2:SOS:Grb2:LAT with a bonding probability (p). Black and gray bonds denote bonding and nonbonding interactions, respectively. Escaping a networked assembly for a LAT molecule requires simultaneous breakage of all bonds. The color gradients represent network sizes that are >10 assembled LAT molecules.

(12). For LAT to form a gel phase, it must be capable of forming a polymer network—the single-molecule tracking of LAT supports that it shares entangled polymerlike features. Given a multivalency of three, LAT can form a macroscopically assembled network if the bonding probability (p) between adjacent LAT (e.g., through the LAT:Grb2:SOS:Grb2:LAT motif) exceeds the critical threshold ($p_c = 1/(f-1)$, where f is the multivalency) (13,14). This is illustrated in Fig. 5. Qualitatively, entanglement of large polymers is prominent near the gel point, suggesting that the reconstituted LAT assemblies are possibly close to that condition.

CONCLUSIONS

Single-molecule tracking of LAT within the phosphotyrosine-mediated assembly reveals a dynamic scaling law similar to that of an entangled polymer. Although the assembly is distinct from a classical polymer in that all of its individual bonds are rapidly breaking and reforming, the mean connectivity within the structure still manifests in a characteristic dynamical scaling law. The elastic feature of LAT assembly is distinctively different from a pure viscous fluid (15). In living cells, subdiffusive motion is commonly observed and often attributed to confinement or crowding effects (33,34). Here, we demonstrate that organization of proteins into networked assemblies leads to timescale-dependent subdiffusion. Moreover, this type of analysis could be performed in live cells (34,35), providing a way of characterizing the molecular-scale organization of visible signaling structures based on dynamics.

SUPPORTING MATERIAL

Supporting Materials and Methods, three figures, and one movie are available at http://www.biophysj.org/biophysj/supplemental/S0006-3495(17)30917-7.

AUTHOR CONTRIBUTIONS

W.Y.C.H. and J.T.G. conceived the study. W.Y.C.H. designed the experiments. W.Y.C.H. and H.-K.C. performed the experiments. W.Y.C.H. analyzed data and carried out the simulations. W.Y.C.H. and J.T.G. wrote the manuscript. J.T.G. supervised the project.

ACKNOWLEDGMENTS

We thank John Kuriyan, Neel Shah, Qingrong Yan, Steven Alvarez, and Young Kwang Lee for reagents and useful discussion.

This work was supported by National Institutes of Health (NIH) National Cancer Institute (NCI) Physical Sciences in Oncology Network Project No. 1-U01CA202241.

REFERENCES

1. Scott, J. D., and T. Pawson. 2009. Cell signaling in space and time: where proteins come together and when they're apart. *Science.* 326:1220–1224.
2. Dustin, M. L., and J. T. Groves. 2012. Receptor signaling clusters in the immune synapse. *Annu. Rev. Biophys.* 41:543–556.
3. Hyman, A. A., and K. Simons. 2012. Cell biology. Beyond oil and water—phase transitions in cells. *Science.* 337:1047–1049.
4. Lowe, A. R., J. H. Tang, …, J. T. Liphardt. 2015. Importin-β modulates the permeability of the nuclear pore complex in a Ran-dependent manner. *eLife.* 4:e04052.
5. Frey, S., R. P. Richter, and D. Görlich. 2006. FG-rich repeats of nuclear pore proteins form a three-dimensional meshwork with hydrogel-like properties. *Science.* 314:815–817.
6. Janes, P. W., E. Nievergall, and M. Lackmann. 2012. Concepts and consequences of Eph receptor clustering. *Semin. Cell Dev. Biol.* 23:43–50.
7. Banjade, S., and M. K. Rosen. 2014. Phase transitions of multivalent proteins can promote clustering of membrane receptors. *eLife.* 3:e04123.
8. Li, P., S. Banjade, …, M. K. Rosen. 2012. Phase transitions in the assembly of multivalent signalling proteins. *Nature.* 483:336–340.
9. Houtman, J. C. D., H. Yamaguchi, …, L. E. Samelson. 2006. Oligomerization of signaling complexes by the multipoint binding of GRB2 to both LAT and SOS1. *Nat. Struct. Mol. Biol.* 13:798–805.

10. Su, X., J. A. Ditlev, …, R. D. Vale. 2016. Phase separation of signaling molecules promotes T cell receptor signal transduction. *Science.* 352:595–599.
11. Huang, W. Y. C., Q. Yan, …, J. T. Groves. 2016. Phosphotyrosine-mediated LAT assembly on membranes drives kinetic bifurcation in recruitment dynamics of the Ras activator SOS. *Proc. Natl. Acad. Sci. USA.* 113:8218–8223.
12. Nag, A., M. I. Monine, …, B. Goldstein. 2009. Aggregation of membrane proteins by cytosolic cross-linkers: theory and simulation of the LAT-Grb2-SOS1 system. *Biophys. J.* 96:2604–2623.
13. Rubinstein, M., and R. H. Colby. 2003. Polymer Physics. Oxford University Press, New York, NY.
14. Flory, P. J. 1941. Molecular size distribution in three-dimensional polymers. I. Gelation. *J. Am. Chem. Soc.* 63:3083–3090.
15. Russel, W. B., D. A. Saville, and W. R. Schowalter. 1989. Colloidal Dispersions. Cambridge University Press, Cambridge, United Kingdom.
16. Houtman, J. C. D., Y. Higashimoto, …, L. E. Samelson. 2004. Binding specificity of multiprotein signaling complexes is determined by both cooperative interactions and affinity preferences. *Biochemistry.* 43:4170–4178.
17. Baumgartner, A. 1984. Simulation of polymer motion. *Annu. Rev. Phys. Chem.* 35:419–435.
18. Izeddin, I., V. Récamier, …, X. Darzacq. 2014. Single-molecule tracking in live cells reveals distinct target-search strategies of transcription factors in the nucleus. *eLife.* 3:e02230.
19. Verdier, P. H., and W. H. Stockmayer. 1962. Monte Carlo calculations on dynamics of polymers in dilute solution. *J. Chem. Phys.* 36: 227–235.
20. Ensign, D. L., and V. S. Pande. 2010. Bayesian detection of intensity changes in single molecule and molecular dynamics trajectories. *J. Phys. Chem. B.* 114:280–292.
21. Rozovsky, S., M. B. Forstner, …, J. T. Groves. 2012. Single molecule kinetics of ENTH binding to lipid membranes. *J. Phys. Chem. B.* 116:5122–5131.
22. Cordes, T., J. Vogelsang, and P. Tinnefeld. 2009. On the mechanism of Trolox as antiblinking and antibleaching reagent. *J. Am. Chem. Soc.* 131:5018–5019.
23. Nye, J. A., and J. T. Groves. 2008. Kinetic control of histidine-tagged protein surface density on supported lipid bilayers. *Langmuir.* 24:4145–4149.
24. Yan, Q., T. Barros, …, J. Kuriyan. 2013. Structural basis for activation of ZAP-70 by phosphorylation of the SH2-kinase linker. *Mol. Cell. Biol.* 33:2188–2201.
25. Condamin, S., V. Tejedor, …, J. Klafter. 2008. Probing microscopic origins of confined subdiffusion by first-passage observables. *Proc. Natl. Acad. Sci. USA.* 105:5675–5680.
26. Lin, W. C., L. Iversen, …, J. T. Groves. 2014. H-Ras forms dimers on membrane surfaces via a protein-protein interface. *Proc. Natl. Acad. Sci. USA.* 111:2996–3001.
27. Chung, J. K., Y. K. Lee, …, J. T. Groves. 2016. Covalent Ras dimerization on membrane surfaces through photosensitized oxidation. *J. Am. Chem. Soc.* 138:1800–1803.
28. Rouse, P. E. 1953. A theory of the linear viscoelastic properties of dilute solutions of coiling polymers. *J. Chem. Phys.* 21:1272–1280.
29. Cates, M. E. 1987. Reptation of living polymers—dynamics of entangled polymers in the presence of reversible chain-scission reactions. *Macromolecules.* 20:2289–2296.
30. Kusumi, A., C. Nakada, …, T. Fujiwara. 2005. Paradigm shift of the plasma membrane concept from the two-dimensional continuum fluid to the partitioned fluid: high-speed single-molecule tracking of membrane molecules. *Annu. Rev. Biophys. Biomol. Struct.* 34:351–378.
31. Dix, J. A., and A. S. Verkman. 2008. Crowding effects on diffusion in solutions and cells. *Annu. Rev. Biophys.* 37:247–263.
32. Degennes, P. G. 1971. Reptation of a polymer chain in presence of fixed obstacles. *J. Chem. Phys.* 55:572–579.
33. Sako, Y., and A. Kusumi. 1994. Compartmentalized structure of the plasma membrane for receptor movements as revealed by a nanometer-level motion analysis. *J. Cell Biol.* 125:1251–1264.
34. Douglass, A. D., and R. D. Vale. 2005. Single-molecule microscopy reveals plasma membrane microdomains created by protein-protein networks that exclude or trap signaling molecules in T cells. *Cell.* 121:937–950.
35. O'Donoghue, G. P., R. M. Pielak, …, J. T. Groves. 2013. Direct single molecule measurement of TCR triggering by agonist pMHC in living primary T cells. *eLife.* 2:e00778.

Biophysical Journal, Volume *113*

Supplemental Information

Dynamic Scaling Analysis of Molecular Motion within the LAT:Grb2:-SOS Protein Network on Membranes

William Y.C. Huang, Han-Kuei Chiang, and Jay T. Groves

Supporting Materials and Methods

Experimental methods and materials used in this study were similar to previous studies (1).

Chemicals

1,2-dioleoyl-sn-glycero-3-phosphocholine (DOPC) and 1,2-dioleoyl-sn-glycero-3-[(N-(5-amino-1-carboxypentyl)iminodiacetic acid)succinyl] (nickel salt) (Ni^{2+}-NTA-DOGS) were purchased from Avanti Polar Lipids. Texas Red 1,2-dihexadecanoylsn-glycero-3-phosphoethanolamine (TR-DHPE) was purchased from Invitrogen. Alexa Fluor 647 maleimide dye and Alexa Fluor 561 maleimide dye were purchased from Life Technology. Bovine Serum Albumin (BSA), (±)-6-Hydroxy-2,5,7,8-tetramethylchromane-2-carboxylic acid (Trolox), Catalase, 2-Mercaptoethanol (BME), $NiCl_2$, H_2SO_4 and ATP were purchased from Sigma-Aldrich. Glucose Oxidase was purchased from Serva. Tris(2-carboxyethyl)phosphine (TCEP) was brought from Thermo Scientific. Glucose and H_2O_2 were from Fisher Scientific. $MgCl_2$ was from EMD Chemicals. Tris buffer saline (TBS) was purchased from Corning.

Protein Purification

LAT, Grb2 and SOS1 are purified similarly to previously work (1, 2). Human LAT cytosolic domain (residues 30 to 233) and full-length Grb2 were purified as described previously (2) using an N-terminal 6-His tag, while proline rich domain of SOS (residue 1051-1333) was purified with similar strategy (1). For both Grb2 and SOS, the N-terminal 6-His tag were removed with Tobacco Etch Virus protease. LAT, Grb2 and SOS were labeled with Alexa Fluor 555, Alexa Fluor 647, Alexa Fluor 647, respectively, using maleimide-thiol chemistry for fluorescently labeled construct.

Protein labeling using maleimide

LAT, Grb2 or SOS were diluted to 100 μM (or less). The proteins were then allowed to react with 1 mM Alexa Fluor 561 or 647 maleimide dye for 2 hrs at room temperature. The reaction was then quenched with 5 mM BME for 10 min. Excess dye was removed by size exclusion chromatography (Superdex 75 (LAT) or Sephadex G-25 (Grb2)).

Functionalized Supported Membranes

Glass substrates (no. 1.5 thickness) were prepared by 5 min piranha etching (H_2SO_4:H_2O_2 = 3:1 by volume), followed by excessive rinsing of H_2O (Milli-Q). Glass substrates were blow dried with air before depositing vesicles to form supported lipid bilayers (SLBs). Small unilamellar vesicles (SUVs) were prepared by mixing DOPC: Ni^{2+}-NTA-DOGS = 96:4 by molar percent in chloroform. If visualization of the bilayers was required, additional 0.005% of TR-DHPE was added to the lipid composition. The solution mixture was then evaporated by a rotary evaporator for 15 min at 40°C. Lipid dried films were further dried with N_2 for another 15 min. The lipids were resuspended in H_2O by vortexing, resulting in a concentration of ~0.5 mg/mL. Finally, the vesicle solution was sonicated with a sonicator for 90 s in an ice-water bath. The membrane system was prepared on a flow chamber (μ-Slid, Ibidi). SLBs were formed on a glass substrate by incubating the SUVs mixed with 40 mM TBS for at least 30 min. The chambers were rinsed with TBS buffer. TBS buffer refers to 20 mM TBS buffer with 5mM $MgCl_2$ at pH 7.4 unless stated otherwise. Next, 1 mg/mL BSA in TBS buffer was incubated for 10 min to block defects in supported membranes. Before protein incubation, the system was buffer exchanged into TBS buffer containing 1 mM TCEP. Proteins were centrifuged for 20 min at 4°C beforehand to remove possible aggregates. Hck and LAT were incubated at 31 and 126 nM, respectively, for 10 min to attach to the bilayers via his-tag Ni^{2+}NTA chemistry (3). The system was allowed to sit for another 20 min to allow unstably bound membrane proteins to dissociate from the surface.

Between all incubation steps, the chambers were rinsed with TBS buffer. Fluidity of the membrane-bound proteins was examined by fluorescent recovery after photobleaching (FRAP). Densities of membrane proteins were estimated by establishing a calibration curve between epifluorescence average intensity and densities measured by fluorescence correlation spectroscopy (FCS) (FCS methods were described previously (4)). LAT assembly was formed by addition of 5.8 μM Grb2, 1.45 μM proline-rich domain of SOS, and 1 mM ATP in scavenger buffer (2 mM UV-treated trolox, 10 mM BME, 20 mM glucose, 320 μg/mL glucose oxidase, 50μg/mL catalase (5)). All parts of preparation were done at room temperature unless otherwise stated.

Single-molecule imaging

Total internal reflection microscopy (TIRF) configuration was setup on a Nikon Eclipse Ti inverted microscopy. TIRF excitations were performed with 561 nm (Sapphire HP, Coherent Inc) laser lines. The optical path was then aligned to a 100x 1.49 NA oil immersion TIRF objective (Nikon). The excitation filter was done with a customized filter optimized for 561 nm (Semrock). The emission was further filtered with 630/75 nm bandpass filter (ET630/75M)). An Andor iXon EMCCD camera was used to record the signals. MetaMorph software (Molecular Devices Corp) was installed to control the microscope. Exposure time was set to 20 ms. Framerate was set to either 2 Hz or 21 Hz. Scavenger buffer for SMT measurements had additional 2 mM UV-treated trolox, 10 mM 2-Mercaptoethanol (BME), 20 mM glucose, 320 μg/mL glucose oxidase, 50 μg/mL catalase and 0.1 mg/mL Bovine Serum Albumin (BSA) in working buffer (5). All analysis were performed on the central 350 by 350 pixel region of the images to minimize uneven illumination. Single-molecule images were analyzed with customized program written in Igor Pro ver. 6.22A (1). The positions and times of LAT trajectories were saved for time-averaging MSD analysis (6): $MSD(n\delta t) = \frac{1}{N-n-1}\sum_{j=1}^{N-n-1}\{[x(j\delta t + n\delta t) - x(j\delta t)]^2 + [y(j\delta t + n\delta t) - y(j\delta t)]^2\}$, where δt is the time between frames, N is the total number of frames in a single trajectory, and n and j are positive integers. The MSD analysis evaluates one trajectory at a time; inspecting many trajectories then provides statistics for various parameters of LAT subdiffusion, such as the characteristic timescales.

Bayesian change-point analysis

The detail derivation of the algorithm is shown in the work by Ensign and Pande (7). In brief, the algorithm evaluates a Bayes factor from a trajectory to describe the likelihood that a change point occurs relative to the likelihood that no change takes place:

$$\text{Bayes Factor} = \frac{P(D|H_2)}{P(D|H_1)} = \frac{|\langle x\rangle|}{2^{\frac{1}{2}}\pi^{\frac{3}{2}}(Ns^2)^{-\frac{N}{2}+\frac{1}{2}}\Gamma(\frac{N}{2}-1)}\left\langle\frac{\prod_{\alpha=1,2}N_\alpha^{-\frac{N_\alpha}{2}+\frac{1}{2}}(s_\alpha^2)^{-\frac{N_\alpha}{2}+1}\Gamma(\frac{N_\alpha}{2}-1)}{(s_1^2+s_2^2)(\langle x_1\rangle^2+\langle x_2\rangle^2)}\right\rangle$$

where D is data, H_1 is no change in the trajectory, H_2 is at least one change in the trajectory, N is the number of data points, s is the standard deviation, the subscripts denotes segment by a changepoint (say t_s is the hypothetic change point, then N_1 is the number of data points prior to t_s and N_2 is the number of data point after t_s), and $\langle\cdot\rangle$ denotes averaging over all possible change-point positions (in the case of Gaussian statistics considered here, it is averaged over $N-5$ values since standard deviation requires at least 3 observables to converge). We chose a threshold Bayes factor of 3 for substantial evidence of a transition occurring within the trajectory if the calculated Bayes factor exceed this value. However, since the degree of freedom in our implementation is the derivative of MSD, it will amplify noise such that the existence of a

change point can be underestimated. Therefore, Bayes factor is just a guideline in this application. The more important application of the algorithm is the estimation of where the transition takes place, based on the posterior distribution of change point positions:

$$P(t_s|D,H_2) \propto \frac{\prod_{\alpha=1,2} N_\alpha^{-\frac{N_\alpha}{2}+\frac{1}{2}} (s_\alpha^2)^{-\frac{N_\alpha}{2}+1} \Gamma(\frac{N_\alpha}{2}-1)}{(s_1^2+s_2^2)(\langle x_1\rangle^2\langle x_2\rangle^2)}$$

The peak of the distribution is where the change point is most likely to occur. The equations used in our analysis are from the Eq. [35] and Eq. [37] of the original work. This analysis can be applied multiple time for multi-change-point detections. After detecting the first (and the most probable) change point, the trajectory is segmented into two fragments by the first change point. We then apply the same algorithm to each of the two fragments for detection of the second change point. This can be repeated multiple time, but in our application, we use it at most twice to evaluate the reptation time and the Rouse time in the LAT trajectories.

Comparison of LAT data with the reptation model

Parameters are calculated by comparing characteristic timescale from single-molecule data of LAT with the reptation model (Fig. 4B). The assignment of the observed timescales to the model is established by recognizing that each scaling follows a particular order ($\tau_{rep} > \tau_R > \tau_e$) with the reptation time τ_{rep} transition from subdiffusive to diffusive motion, i.e. the slowest characteristic timescale in Fig. 2 will correspond to τ_{rep}. Next, this mapping, along with relations in the reptation model gives the following equations (Fig. 4B):

Reptation time $\tau_{rep} = 6\tau_0 N_e^2 \left(\frac{N}{N_e}\right)^3 = 5.1\ s$ Eq. [1]

Rouse time $\tau_R = \tau_0 N^2 = 0.64\ s$ Eq. [2]

Rouse time of entangled strand $\tau_e = \tau_0 N_e^2$=not observed due to resolution limit(~100ms) Eq. [3]

where N_e is number of monomers in an entangled strand, N is the total number of monomers in the polymer, τ_0 is the monomer relaxation time. Although these equations cannot solve for all variables, we can calculate the ratio of N/N_e and τ_e. By dividing Eq. [1] by Eq. [2], $N/N_e \sim 1.3$. Inserting this result back to Eq. [1] gives $\tau_e \sim 300$ ms.

Monte Carlo simulations

The main purpose of the simulations is to show that different subdiffusion mechanism may be distinguishable from experimental MSD analyses. For this purpose, we consider the simplest case for each mechanism. All simulations initiate with a particle in infinite 2D squared lattices. In each step of random walk simulation, the particle randomly moved along one axis of the lattices. The positions and times of each step were saved and analyzed following the same MSD analysis in the experiments. Since the goal is to inspect the qualitative shape of MSD for each mechanism, most parameters are arbitrary chosen such that the shape of MSD are resolved within the simulation time. All simulations were performed in Matlab R2016a.

Polymer constraints

The algorithm for simulating subdiffusion of a polymer largely follows Verdier-Stockmayer model (8-10). The tagged molecules belongs to a polymer of $N = 20$ beads (we chose an intermediate size polymer since a larger size requires longer simulation time and a short polymer has subdiffusion only at a very fast timescale). We consider the simpliest case of polymer

network since the structural orientation of LAT is unknown (an intrinsically disordered protein) – a non self-avoiding polymer on a 2D lattices by itself. The network is initiated by randomly orienting the polymer bonds on a 2D lattices. Occasionly, this leads to an immobile network, which we discard. Then, the polymer moves according to the rules described in Verdier-Stockmayer model. During each time unit of $1/N$, a random monomer in the network is chosen to move. The local bond geometry of the tagged paricle is examined to determine legal movements. There are three types of allowed motions: ***i)*** if the two adjacent bonds connecting the particle are perpendicular to each other, the particle then moves to opposite corner such that both of the bonds are flipped by 90 degree – referred to as "coner move", ***ii)*** if the two adjacent bonds are overlapping each other, the particle will randomly redirect both of the bonds – referred to as "kink jump", and, ***iii)*** if the bead at either end point, it reorient the single bonds randomly. Any other type of motions were restricted by bond constraints in the simulations. A schematic for the described allowed motions are shown in p. 391 in Rubinstein and Colby, *Polymer Physics* (10).

Confinement

The particle follows standard random walk described earlier, except that the 2D lattices are confined in a 20 by 20 unit impassable square box (the length of the confinement is chosen to result in a similar timescale to polymer constraints). If the particle randomly attempt to cross the boundary, it will remain at the same spot. This exemplify the case of picket-and-fence model commonly discussed in the plasma membrane.

Crowding effect

We consider the case of crowding in a dynamic environment using continuous time random walk, following the work by Condamin (11). After the tagged particle moving to a new position, the molecule is trapped with a waiting time following a heavy-tail probability distribution (11, 12): $P(1 < T < t) = 1 - t^{-\alpha}$, and $P(T < 1) = 0$. α was chosen to be 0.5.

Bond dynamics

The effect of pure bond dynamics is considered by having the tagged particle randomly binding to immobile sites on 2D lattices (Fig. 3D). Each time the particle move to a new position, we set a probability of 0.2 to become engaged in an immobile site for a 200-unit lifetime (chosen to compare with the characteristic timescale of polymer motion). This represent the case where the molecular motions from binding-and-rebinding greatly exceed that of local movement of the network. Binding to a mobile polymer network (Fig. 3E) is evaluated similarly except that the bond lifetime is 50 or 500 unit (depending on whether we are looking at short or long bond lifetime). During the bond lifetime, the particle resumes the motion as described in polymer constraints.

Reference

1. Huang, W. Y. C., Q. Yan, W. C. Lin, J. Chung, S. D. Hansen, S. M. Christensen, H. L. Tu, J. Kuriyan, and J. T. Groves. 2016. Phosphotyrosine-mediated LAT assembly on membranes drives kinetic bifurcation in recruitment dynamics of the Ras activator SOS. Proc. Natl. Acad. Sci. USA 113:8218-8223.
2. Yan, Q., T. Barros, P. R. Visperas, S. Deindl, T. A. Kadlecek, A. Weiss, and J. Kuriyan. 2013. Structural basis for activation of ZAP-70 by phosphorylation of the SH2-kinase linker. Mol. Cell. Biol. 33:2188-2201.
3. Nye, J. A., and J. T. Groves. 2008. Kinetic control of histidine-tagged protein surface density on supported lipid bilayers. Langmuir 24:4145-4149.
4. Lin, W. C., L. Iversen, H. L. Tu, C. Rhodes, S. M. Christensen, J. S. Iwig, S. D. Hansen, W. Y. C. Huang, and J. T. Groves. 2014. H-Ras forms dimers on membrane surfaces via a protein-protein interface. Proc. Natl. Acad. Sci. USA 111:2996-3001.
5. Cordes, T., J. Vogelsang, and P. Tinnefeld. 2009. On the Mechanism of Trolox as Antiblinking and Antibleaching Reagent. J. Am. Chem. Soc. 131:5018-5019.
6. Rozovsky, S., M. B. Forstner, H. Sondermann, and J. T. Groves. 2012. Single Molecule Kinetics of ENTH Binding to Lipid Membranes. J. Phys. Chem. B 116:5122-5131.
7. Ensign, D. L., and V. S. Pande. 2010. Bayesian Detection of Intensity Changes in Single Molecule and Molecular Dynamics Trajectories. J. Phys. Chem. B 114:280-292.
8. Verdier, P. H., and W. H. Stockmayer. 1962. Monte Carlo Calculations on Dynamics of Polymers in Dilute Solution. J. Chem. Phys. 36:227-+.
9. Baumgartner, A. 1984. Simulation of Polymer Motion. Annu. Rev. Phys. Chem. 35:419-435.
10. Rubinstein, M., and R. H. Colby. 2003. Polymer Physics. Oxford University Press, New York, U.S.A.
11. Condamin, S., V. Tejedor, R. Voituriez, O. Benichou, and J. Klafter. 2008. Probing microscopic origins of confined subdiffusion by first-passage observables. Proc. Natl. Acad. Sci. USA 105:5675-5680.
12. Izeddin, I., V. Recamier, L. Bosanac, I. I. Cisse, L. Boudarene, C. Dugast-Darzacq, F. Proux, O. Benichou, R. Voituriez, O. Bensaude, M. Dahan, and X. Darzacq. 2014. Single-molecule tracking in live cells reveals distinct target-search strategies of transcription factors in the nucleus. eLife 3:e02230.

Supporting Figures

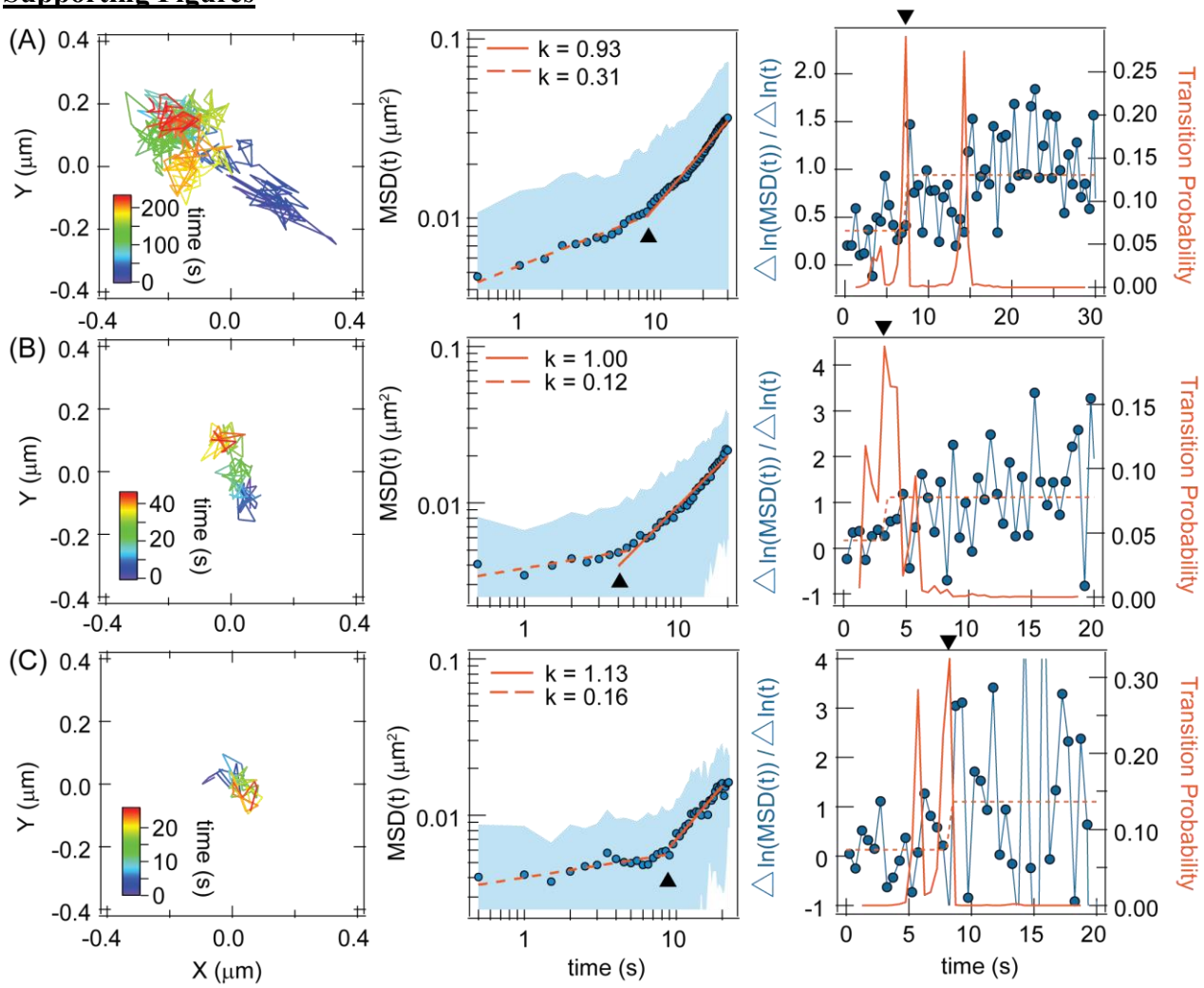

FIGURE S1. Additional examples of LAT subdiffusion. Single-molecule tracking of dilute labeled LAT within assemblies, time-averaging MSD analysis, and Bayesian change-point analysis are shown in the left, middle, and right column, respectively. The time axis is color coded in the trajectory. Time-averaging MSD plots are fitted to a power law in log-log plot. Shaded area is the standard deviation of statistics from a single trajectory. The fitted $\{A_{k\sim1}, A_{k<1}\}$ for top, middle, and bottom MSD are {0.0015, 0.0054}, {0.00098, 0.0039}, and {0.00052, 0.0040}, respectively.

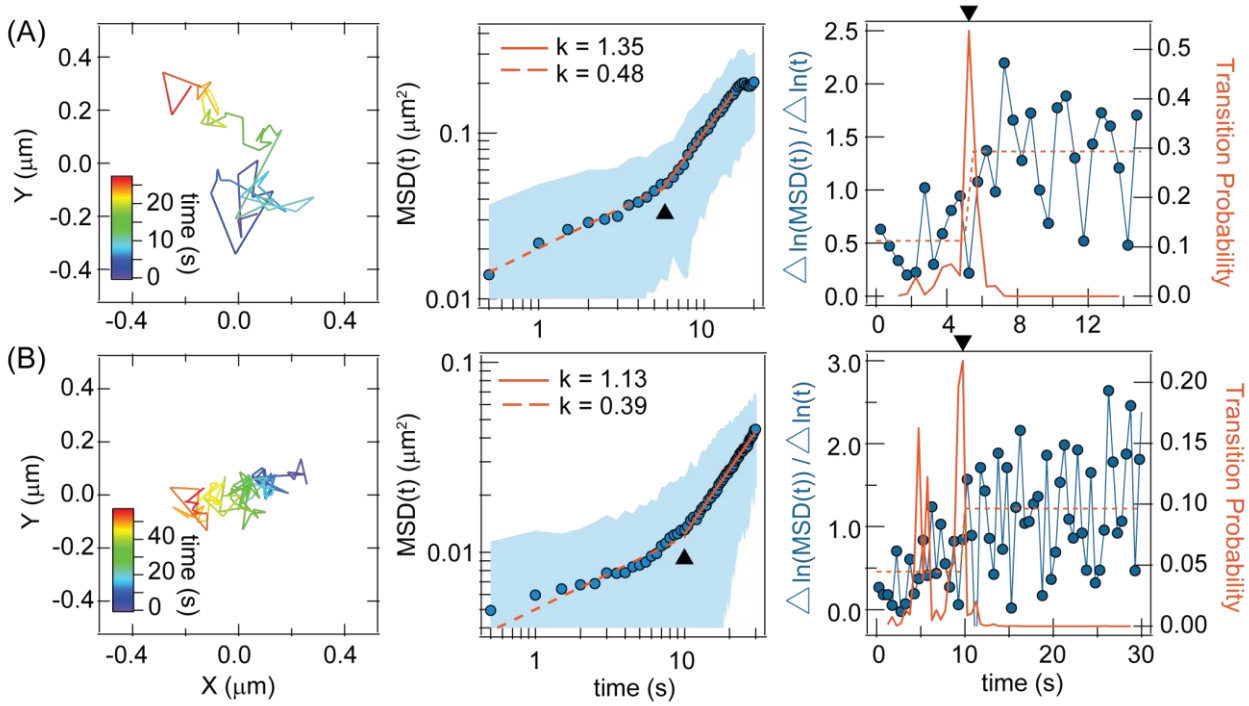

FIGURE S2. Time-dependent subdiffusion of Grb2 and SOS. Representative examples of Grb2 (top) and SOS (bottom) trajectory analysis within assembly structure. The long dwell times of Grb2 and SOS reflect their multivalent interactions with the assemblies (1). The time axis is color coded in the trajectory. Time-averaging MSD plots are fitted to a power law in log-log plot. Shaded area is the standard deviation of statistics from a single trajectory. The fitted $\{A_{k\sim1}, A_{k<1}\}$ for Grb2 and SOS are {0.0045, 0.020} and {0.00090, 0.0050}, respectively.

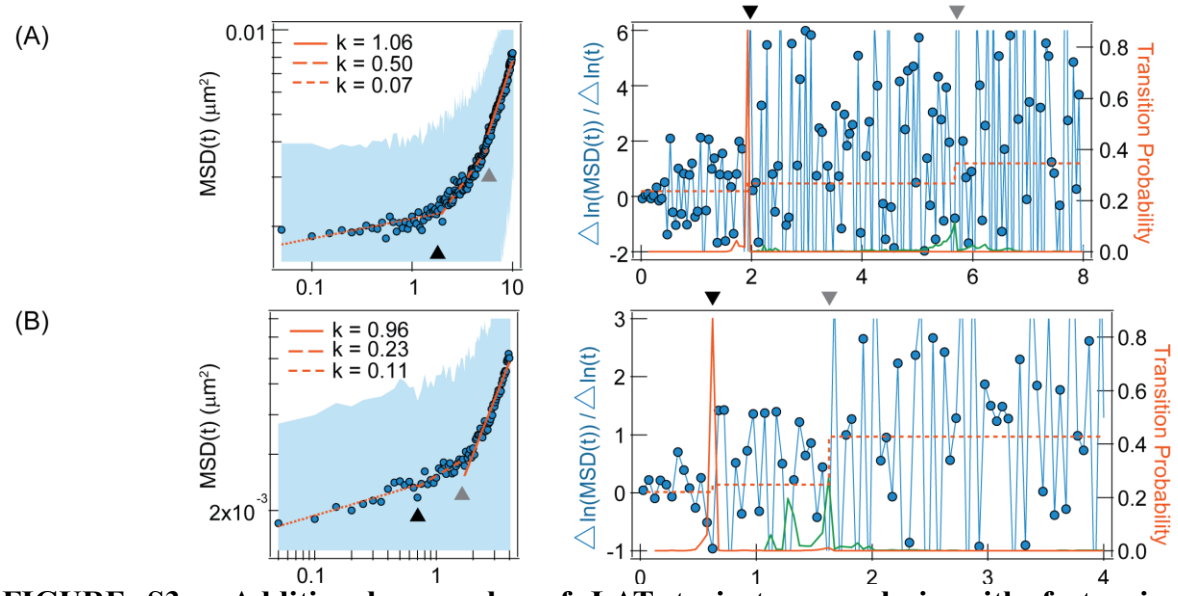

FIGURE S3. Additional examples of LAT trajectory analysis with faster imaging acquisition. MSD analysis of LAT mobility acquired at a framerate of 21 Hz. Shaded area is the standard deviation of statistics from a single trajectory. Each timescale is fitted by a power law, with the characteristic timescales denoted by triangles. The fitted A for $k = 1.06,0.50,0.07,0.96,0.23,0.11$ are 0.00067, 0.0015, 0.002, 0.0016, 0.0027, and 0.0025, respectively. The orange and green curve of the right plot corresponds to the transition probability calculated from the full timescale and the partial timescale after to the faster (black triangle) characteristic timescale, respectively.

Supporting Movie

Movie S1. Single-molecule imaging of LAT. Imaging of LAT-Alexa Flour 555 at a frame rate of 2 Hz. Most of the particles are mobile over longer timescales (>10 s).